Journal of Solid State Chemistry **163,** 479–483 (2002)
doi:10.1006/jssc.2001.9431, available online at http://www.idealibrary.com on IDEAL®

Microstructures of Some Bi–W–Nb–O Phases

Wuzong Zhou[1]

School of Chemistry, University of St. Andrews, St. Andrews, Fife KY16 9ST, United Kingdom

Received July 17, 2001; in revised form October 8, 2001; accepted October 15, 2001

Microstructures of three Bi–W–Nb–O phases have been examined by using high-resolution transmission electron microscopy. $Bi_{17}W_2Nb_3O_{39}$ and $Bi_{17}WNb_3O_{36}$ have incommensurate superstructures derived from the defect fluorite-type δ-Bi_2O_3 and can be regarded as intermediate phases between the type II solid solutions in the Bi–Nb–O and Bi–W–O systems. $Bi_8W_2Nb_2O_{23}$ has a Bi_2WO_6-like subunit cell with a stepped superstructure. Formation mechanisms of various superstructures are discussed.

Key Words: **transmission electron microscopy; $Bi_{17}W_2Nb_3O_{39}$; $Bi_{17}WNb_3O_{36}$; incommensurate superstructures; Bi_2O_3; solid solutions; $Bi_8W_2Nb_2O_{23}$; Bi_2WO_6.**

INTRODUCTION

Defect fluorite Bi_2O_3-based solid solutions and Aurivillius phases containing fluorite-type Bi_2O_2 layers have attracted increasing attention in the past few years as a result of their excellent oxide ionic conductive (1, 2) and ferroelectric properties (3).

Fluorite-type δ-Bi_2O_3 is a high-temperature phase and contains 25% oxygen vacancies. It is therefore easy to introduce guest metal oxides with $4+$ or higher charge valence of the cations into the structure to form solid solutions. Consequently, the concentration of the oxygen vacancies is reduced and the structure can be stabilized at room temperature (4). The Aurivillius phases (5) have a general formula, $[Bi_2O_2][A_{n-1}B_nO_{3n+1}]$ (where the B sites are usually occupied by transition metal cations), composed of fluorite-type $[Bi_2O_2]$ layers and perovskite-type $[A_{n-1}B_nO_{3n+1}]$ blocks.

In the author's previous work, the detailed structural chemistry of the ternary oxide systems of Bi–Nb–O and Bi–W–O was investigated by using high-resolution transmission electron microscopy (HRTEM) (4, 6–8). It was confirmed that both WO_3 and Nb_2O_5 acted as solutes in the δ-Bi_2O_3 matrix and stabilized the structure at room temperature. As their concentrations increased, guest oxides formed isolated MO_6 octahedra in the type I superstructures, and pyrochlore-type M_4O_{18} clusters in type II superstructures (M = W or Nb). The HRTEM method is not sensitive to light elements, such as oxygen. Using X-ray and neutron diffraction methods, it was proposed that some of the oxygen sites in WO_6 octahedra are only partially occupied, resulting in highly distorted tetrahedral coordination for W in the type I superstructure (9, 10). A similar result was also observed from $Bi_{14}CrO_{24}$ when the coordination of Cr was considered (11). In addition, new M–O units, e.g., strings of MO_6 octahedra, were believed to exist three-dimensionally in the type II superstructure (9, 12, 13), although such string units did not give good image matching during the author"s HRTEM image simulations (4).

The δ-Bi_2O_3-based structure transformed into Aurivillius phases when the compositions reached Bi_2WO_6 and $Bi_{15}Nb_3O_{15}$, respectively. The former is an $n=1$ member of Aurivillius phase and the latter is a regular intergrown phase of $\{[Bi_2O_2][NbO_4]\}^-$ ($n=1$) and $\{[Bi_2O_2][BiNb_2O_7]\}^+$ ($n=2$). One extraordinary property of the Aurivillius phases is that all transition metal cations in the structures are at their highest stable oxidation state, such as W^{6+}, Nb^{5+}, Ti^{4+}, etc, and it seems to be very difficult to partially reduce these cations when the Aurivillius structure is still maintained (14). Cation substitution at a very low level for introducing oxygen vacancies was proved to be possible by Baux *et al*., who used niobium to replace up to 15% tungsten in Bi_2WO_6 and the defect Aurivillius phase showed good oxide ion conductivity (15, 16). The ion-conducting property was destroyed by further substitution of niobium, implying a possible structural change. Nevertheless, structural modifications of the Auvillius phases by chemical substitutions, introducing oxygen vacancies in order to achieve high oxygen ion conductivity, have attracted increased efforts in recent years (17–19).

Because both W and Nb cations likely form similar clusters in the δ-Bi_2O_3 matrix, it is of interest to investigate some intermediate Bi–W–Nb–O phases, which has not been studied extensively except that a stepped superstructure based on Bi_2WO_6 was mentioned previously. (14, 20). In the

[1]Fax: 01334-463808. E-mail: wzhou@st-andrews.ac.uk.

0022-4596/02 $35.00

present work, $Bi_{17}W_2Nb_3O_{39}$, $Bi_{17}WNb_3O_{36}$, and $Bi_8W_2Nb_2O_{23}$ were synthesized and their detailed structures investigated by HRTEM.

EXPERIMENTAL

Specimens were prepared from the starting materials Bi_2O_3 (99.9%), Nb_2O_5 (99.9%), and WO_3 (99.99%), by solid state reaction with cation ratios Bi:W:Nb of 17:1:3, 17:2:3, and 4:1:1. The mixed oxides were ground with acetone in an agate mortar and pestle for a few minutes. For the compositions of 17:1:3 and 17:2:3, the specimen was placed in a silica boat and heated in a pure oxygen atmosphere at 900°C for 24 hours, followed by quenching to room temperature. The 4:1:1 specimen was synthesized under the same conditions except the heating temperature was 50°C higher.

Initial characterization of the specimens was by X-ray powder diffraction (XRD). Chemical compositions of the samples were examined by using energy dispersive X-ray (EDX) spectrometry. A molybdenum specimen grid was placed in a graphite grid holder and graphite slurry was used to cover the metal part of the specimen holder near the grid. Therefore, the intensity of the Cu$K\alpha$ emission line was then greatly reduced without detectable overlap with the W $L\alpha$ line. Selected area electron diffraction (SAED) patterns and HRTEM images were recorded from a Jeol JEM-200CX electron microscope, in which a modified side-entry specimen stage with objective lens parameters $C_s = 0.52$ mm and $C_c = 1.05$ mm was used, and the corresponding absolute information limit is about 0.18 nm (21).

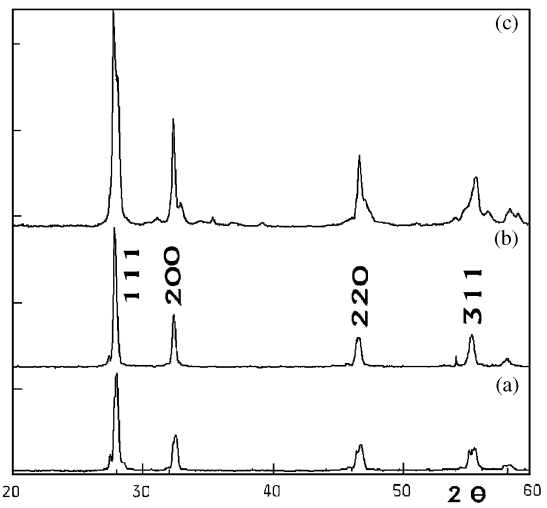

FIG. 1. XRD patterns of (a) $Bi_{17}W_2Nb_3O_{39}$, (b) $Bi_{17}WNb_3O_{36}$, and (c) $Bi_8W_2Nb_2O_{23}$. (b) is indexed onto a fluorite-like subunit cell with $a \approx 0.55$ nm.

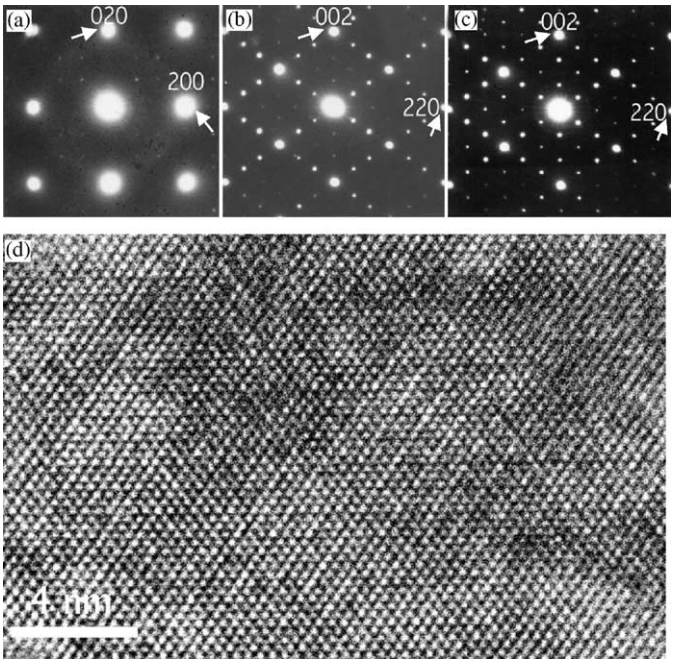

FIG. 2. SAED patterns of $Bi_{17}WNb_3O_{36}$ viewed down the (a) [001] and (b) [1$\bar{1}$0] zone axes. (c) SAED pattern of $Bi_{17}W_2Nb_3O_{39}$ along the [1$\bar{1}$0] direction and (d) the corresponding HRTEM image. All the SAED patterns are indexed onto the fluorite-type subcell.

RESULTS AND DISCUSSION

XRD patterns of the synthesized specimens can be indexed onto a fluorite-like cubic unit cell or a distorted tetragonal unit cell with the unit cell dimensions of about 0.55 nm (Fig. 1).

Using freshly prepared and monophasic $BiNbO_4$ and Bi_2WO_6 as reference materials, 20 particles from each sample were examined by EDX. Based on calculation of the intensity ratio of Bi$L\alpha$:W$L\alpha$:Nb$K\alpha$, it was revealed that the specimens were almost homogeneous with some particles, in which W and Nb contents were slightly variable while the ratio of Bi to (W + Nb) remained the same.

SAED patterns and HRTEM images from $Bi_{17}WNb_3O_{36}$ show a structure similar to type II solid solution in the Bi_2O_3–Nb_2O_5 system. Two principal SAED patterns of the compound are shown in Figs. 2a and 2b. The real structure of the type II Bi–Nb–O is incommensurate and the compositional range of this solid solution is from $Bi_{24}Nb_2O_{41}$ to Bi_3NbO_7. The best commensurate model approaching the real structure was developed on the basis of computer simulations of the SAED patterns and HRTEM images. It has an $8 \times 8 \times 8$ supercell derived from δ-Bi_2O_3 and the cell composition of $Bi_{1648}Nb_{400}O_{3472}$ is close to $Bi_8Nb_2O_{17}$ (4, 22). In the structure, niobium exists in two types of pyrochlore-type clusters, Nb_7O_{30} and $Nb_{18}O_{72}$, that are ordered or partially ordered in the δ-Bi_2O_3 matrix.

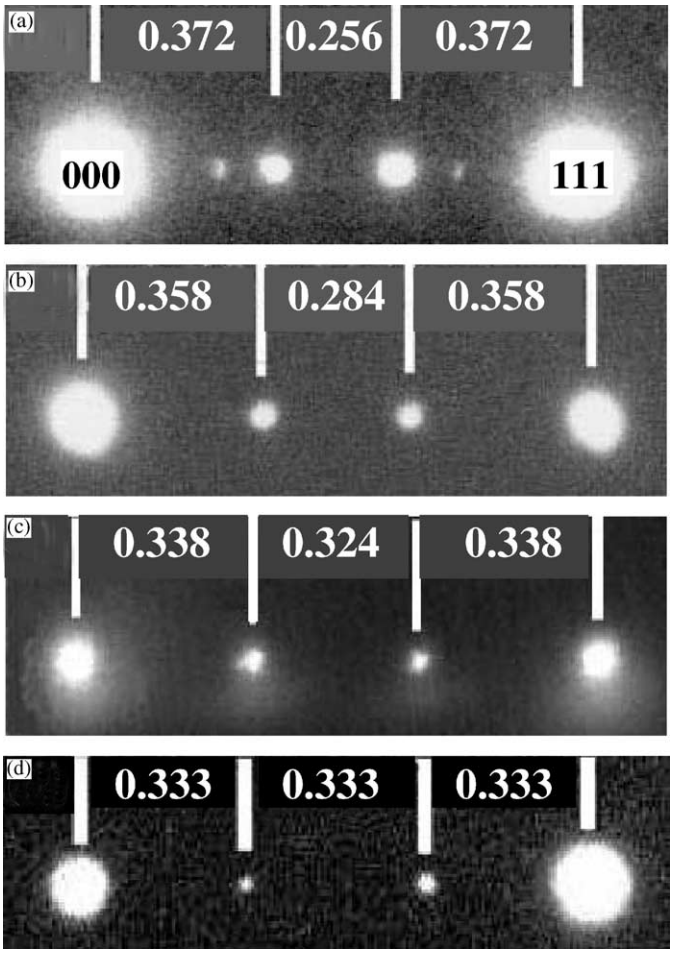

FIG. 3. SAED spots along the [111] direction of the fluorite-like subcell from (a) $Bi_8Nb_2O_{17}$, (b) $Bi_{17}WNb_3O_{36}$, (c) $Bi_{17}W_2Nb_3O_{39}$, and (d) $Bi_{10}W_2O_{21}$. The relative positions of the superstructural diffraction spots are indicated.

These clusters can be regarded as combinations of two and six Nb_4O_{18} tetrahedral clusters by sharing one and six Nb cations, respectively. The type II solid solution in the Bi_2O_3–WO_3 system, however, has a commensurate $3 \times 3 \times 3$ superstructure and covers a compositional range from Bi_6WO_{12} to Bi_4WO_9 (8). Tungsten cations form simple tetrahedral W_4O_{18} clusters in the δ-Bi_2O_3 matrix. Consequently, all the clusters mentioned above were expected to be present in $Bi_{17}WNb_3O_{36}$, leading to an intermediate phase between the type II phases in the Bi–Nb–O and Bi–W–O systems.

To prove the above hypothesis, it is worth comparing the positions of superstructural diffraction spots in the SAED patterns obtained from the relevant samples. Figure 3a shows that the position of the principal supercell diffraction spot along the [111] direction of $Bi_8Nb_2O_{17}$ is 0.372 of the corresponding distance of the (111) spot, indicating an incommensurate superstructure. On the other hand, the value of 0.372 is very close to $\frac{3}{8}$ and, therefore, it could be indexed as the (333) diffraction spot to the $8 \times 8 \times 8$ superunit cell. The corresponding distance in the SAED pattern of Bi_4WO_9 is 0.333, showing a $3 \times 3 \times 3$ commensurate superlattice (Fig. 3d), and that from $Bi_{17}WNb_3O_{36}$ is 0.358, falling in between the former two (Fig. 3b).

Both the SAED patterns and HRTEM images from $Bi_{17}W_2Nb_3O_{39}$ show a structure similar to the type II structure in the Bi–W–O system (Figs. 2c and 2d) (8). The superstructure is still incommensurate and the measurement of the positions of the supercell diffraction spots confirms that it can be regarded as an intermediate phase between $Bi_{17}WNb_3O_{36}$ and Bi_4WO_9 (Fig. 3c).

Although the Nb–O and W–O clusters in the δ-Bi_2O_3 matrix are different, resulting in incommensurate and commensurate superstructures, respectively, the basic units of these clusters are the same, namely tetrahedral M_4O_{18} (M = Nb or W). The clusters can be homogeneously mixed in the δ-Bi_2O_3 matrix if the specimens are quenched to room temperature. In the obtained HRTEM images, no domain structure was observed. However, it was noticed that the type II solid solution phases containing both W and Nb become relatively unstable in comparison with the ternary Bi–Nb–O or Bi–W–O specimens. Under electron beam irradiation for a few minutes, decomposition could be observed from the particles of both $Bi_{17}WNb_3O_{36}$ and $Bi_{17}W_2Nb_3O_{39}$.

The XRD result of $Bi_8W_2Nb_2O_{23}$ (Fig. 1c) also indicates a fluorite-like structure rather than a Bi_2WO_6-type phase, although some weak peaks, which are probably reflected from the Bi_2WO_6-like phase, are visible. The (004) peak of the Bi_2WO_6 phase at about 22° of 2θ is missing and the

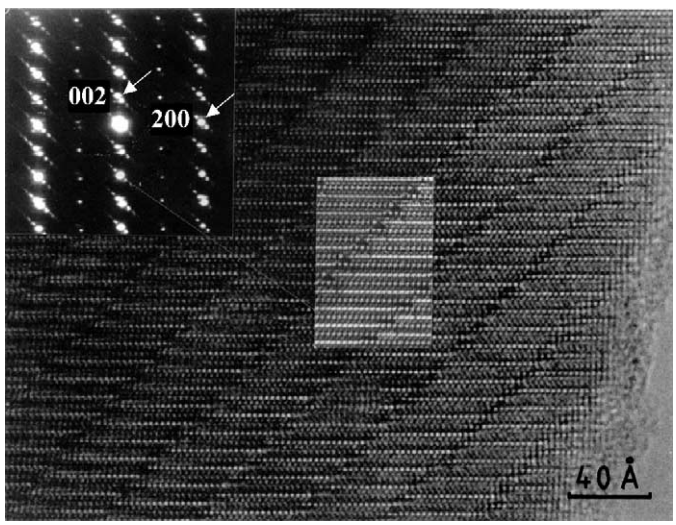

FIG. 4. HRTEM image of $Bi_8W_2Nb_2O_{23}$ viewed down the [010] zone axis of a Bi_2WO_6-like subcell. The insets show a corresponding SAED pattern (top) and a simulated image from a proposed model with 8-nm specimen thickness and 60-nm lens defocus (10).

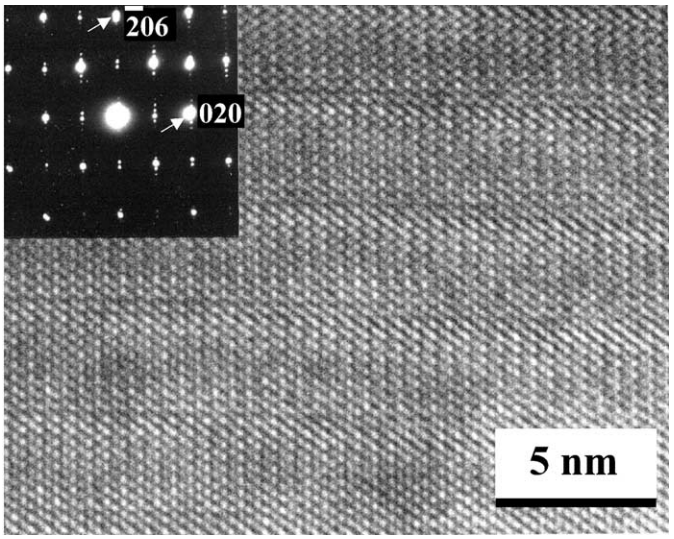

FIG. 5. HRTEM image of $Bi_8W_2Nb_2O_{23}$ viewed down the [301] zone axis of the Bi_2WO_6-like subcell. The principal diffraction spots are indexed onto the subcell.

intensity of the (006) peak close to the (200) peak of the fluorite phase (Fig. 1b) reduces dramatically (23).

On the other hand, the material can be regarded as $n = 1$ Aurivillius phase, Bi_2WO_6, with 50% W replaced by Nb. HRTEM images indeed show a Bi_2WO_6-like structure, having a basic tetragonal unit cell with $a = 0.545$ nm and $c = 1.749$ nm. The reason for the great variation of the XRD pattern is that a perfect Bi_2WO_6-like structure does not exist. All the crystallites show a stepped superstructure, which was first reported by Jefferson in 1985 (20) and further studied by the author in 1990 (14). Figure 4 is a HRTEM image of $Bi_8W_2Nb_2O_{23}$ along the [010] direction. A stepped structure forms by shifting half a unit cell on the $(\bar{1}03)$ planes. Figure 5 shows a HRTEM image of the specimen viewed down the [301] zone axis of the Bi_2WO_6-like subcell, revealing that no superlattice presents along the [010] zone axis. Both images and corresponding SAED patterns in Figs. 4 and 5 indicate that the longest superunit cell axis is along the $[\bar{1}03]$ direction of the subcell. A model of the superstructure has been then proposed, which is monoclinic with $a = 7.903$, $b = 0.545$, and $c = 1.197$ nm and $\beta = 133.07°$ (Fig. 6). Using this model, computer-simulated images can match the experimental ones very well (Fig. 4).

The formation mechanism of this stepped superstructure is that, when Nb substitutes W in Bi_2WO_6, the interlayer electrical charge balance of $Bi_2O_2^{2+}$ and WO_4^{2-} is disturbed. A combination of the $Bi_2O_2^{2+}$ and NbO_4^{3-} layers does not fit a neutral component in a half unit cell scale. Alternatively, to achieve an electrical charge balance, some oxygen vacancies must be introduced into the structure. However, both the loss of interlayer charge balance and the presence of oxygen vacancies would be unfavorable for maintaining the Aurivillius structure. A stepped superstructure can more or less overcome these problems. First, the electrical charge separation along the c direction can be greatly reduced. Second, at the corners of the steps, fewer oxygen atoms may be required. For example, the proposed model in Fig. 6 contains some small $n = 2$ Aurivillius components and has a composition of $Bi_{60}M_{30}O_{174}$ (M = W and Nb) instead of the composition of $Bi_{60}M_{30}O_{180}$ corresponding to a perfect Bi_2WO_6 structure.

The model shown in Fig. 6 demonstrates the principle of the superstructural formation and is approaching the real structure. In fact, the microstructure of $Bi_8W_2Nb_2O_{23}$ is even more complex. First, the [100] dimension of the superunit cell is variable, sometimes making the supercell incommensurate. Second, the c axis of the supercell can be parallel to the [103] as well as to the $[\bar{1}03]$ zone axis of the subcell and these two possible orientations of the monoclinic superlattice coexist in most particles to form twin defects or a zigzag superstructure (Fig. 7) Finally, the $[Bi_2O_2]$ components in Bi_2WO_6 phase and in $Bi_8W_2Nb_2O_{23}$ are the same: a fluorite type. Intergrowths between $Bi_8W_2Nb_2O_{23}$ and Bi_2WO_6, and between

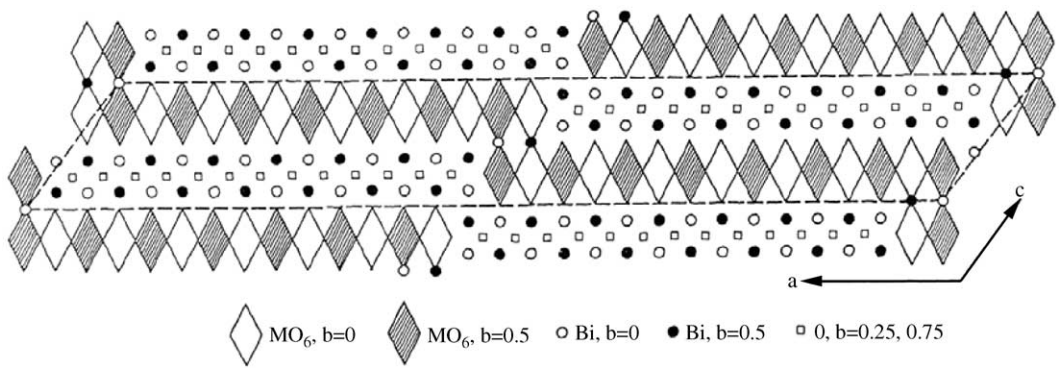

FIG. 6. A stepped superstructural model of $Bi_8W_2Nb_2O_{23}$. The M sites are shared by W and Nb.

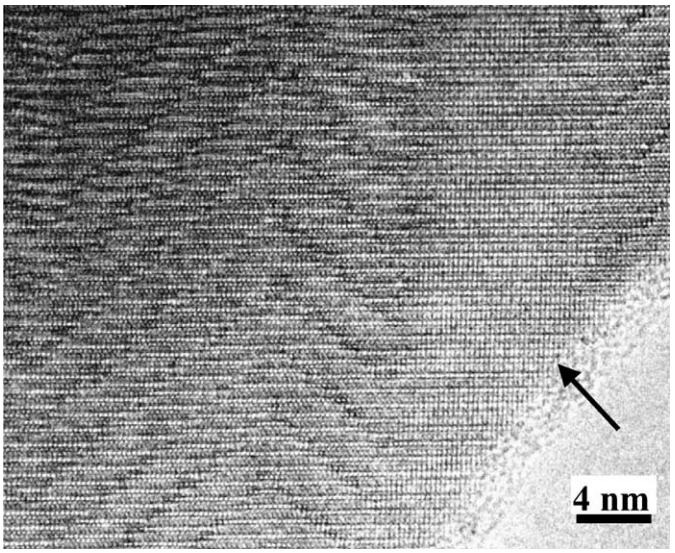

FIG. 7. HRTEM image from $Bi_8W_2Nb_2O_{23}$ viewed down the [010] direction. A zigzag secondary superstructure is presented. The domain indicated by an arrow is Bi_2WO_6.

$Bi_8W_2Nb_2O_{23}$ and the type II solid solution phase, were occasionally observed in the synthesized $Bi_8W_2Nb_2O_{23}$ specimen. As seen in Fig. 7, $Bi_8W_2Nb_2O_{23}$ and Bi_2WO_6 phases can intergrow together on the (100) planes of the subcell, but no grain boundaries can be easily distinguished.

Figure 8 shows an intergrowth between $Bi_8W_2Nb_2O_{23}$ and the type II solid solution phase. The intergrowth planes are the $(\bar{1}03)$ of $Bi_8W_2Nb_2O_{23}$ and the (110) of the type II structure. The atomic arrangements on these two planes are quite similar and again no clear boundaries can be identified.

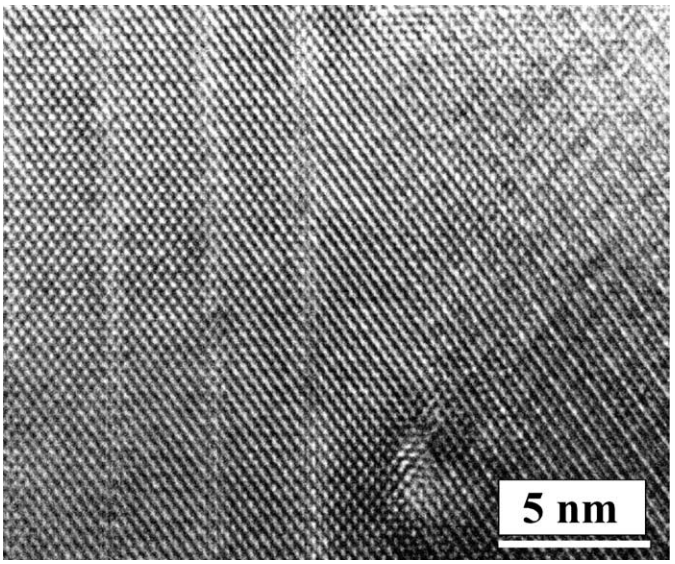

FIG. 8. HRTEM image showing an intergrowth between $Bi_8W_2Nb_2O_{23}$ (left) and a type II solid solution phase (right). The projections of the two phases are the same as those in Figs. 5 and 2d, respectively.

In summary, various concentrations of W and Nb can coexist in the δ-Bi_2O_3 matrix to stabilize the structure. When the cation ratio Bi:(W, Nb) fits those of the type II solid solutions, the specimen has an incommensurate superstructure and can be regarded as an intermediate phase between the type II structures in the Bi–Nb–O and Bi–W–O systems. A large amount of W in Bi_2WO_6 can be replaced by Nb. A stepped superstructure forms based on the $n = 1$ Aurivillius structure. Some zigzag secondary superstructures are commonly presented. Since all the phases discussed in the present work contain fluorite-type bismuth oxide components, intergrowths of these phases can be easily formed.

ACKNOWLEDGMENTS

The author thanks Dr. D. A. Jefferson for his many valuable discussions.

REFERENCES

1. J. A. Kilner and B. C. H. Steele, *in* "Non-stoichiometric oxides" (O. T. Sorensen, Ed.), Chap. 5, Academic Press, New York, 1981.
2. N. Baux, R. N. Vannier, G. Mairesse, and G. Nowogrocki, *Solid State Ionics* **91,** 243(1996).
3. C. A. P. de Araujo, J. D. Cuchlaro, L. D. McMillan, M. C. Scott, and J. F. Scott, *Nature* **374,** 627 (1995).
4. W. Zhou, D. A. Jefferson, and J. M. Thomas, *Proc. R. Soc. London. A* **406,** 173 (1986).
5. B. Aurivillius, *Arkiv. Kemi* **1,** 463 (1949).
6. W. Zhou, D. A. Jefferson, and J. M. Thomas, *J. Solid State Chem.* **70,** 129 (1987).
7. W. Zhou, D. A. Jefferson, and J. M. Thomas, "Perovskite: A Structure of Great Interest to Geophysics and Materials Science" (A. Navrotsky and D. J. Weidner, Eds.), Geophys. Monograph **45,** p. 113. American Geophysical Union, Washington D.C., 1989.
8. W. Zhou, *J. Solid State Chem.* **108,** 381 (1994).
9. C. D. Ling, *J. Solid State Chem.* **148,** 380 (1999).
10. C. D. Ling, R. L. Withers, L. G. Thompson, and S. Schmid, *Acta. Crystallogr. B* **55,** 306(1999).
11. S. A. Warda, W. Pietzuch, W. Massa, U. Kesper, and D. Reinen, *J. Solid State Chem.* **149,** 209 (2000).
12. R. L. Withers, C. D. Ling, and S. Schmid, *Z. Krist.* **214,** 296 (1999).
13. S. Esmaeilzadeh, S. Lundgren, U. Halenius, and J. Grins, *J. Solid State Chem.* **156,** 168(2001).
14. W. Zhou, *Adv. Mater.* **2,** 94 (1990).
15. N. Baux, R. N. Vannier, G. Mairesse, and G. Nowogrocki, *Solid State Ionics* **91,** 243 (1996).
16. M. S. Islam, S. Lazure, R. N. Vannier, G. Nowogrocki, and G. Mairesse, *J. Mater. Chem.* **8,** 655 (1998).
17. A. Castro, P. Millan, and R. Enjalbert, *Mater. Res. Bull.* **30,** 871 (1995).
18. K. R. Kendall, C. Navas, J. K. Thomas, and H.-C. zur Loye, *Chem. Mater.* **8,** 642 (1996).
19. K. R. Kendall, J. K. Thomas, and H.-C. zur Loye, *Chem. Mater.* **7,** 50 (1995).
20. D. A. Jefferson, *Am. Chem. Soc. Symp. Ser.* **11,** 183 (1985).
21. D. A. Jefferson, J. M. Thomas, G. R. Millward, K. Tsuno, A. Harriman, and R. D. Brydson, *Nature* **323,** 428 (1986).
22. D. Tang and W. Zhou, *J. Solid State Chem.* **119,** 311 (1995).
23. A. Watanabe, *Mater. Res. Bull.* **19,** 877 (1984).